

M.S. Reis* and V.S. Amaral

Departamento de Física and CICECO, Universidade de Aveiro, 3810-193 Aveiro, Portugal

J.P. Araújo

IFIMUP, Departamento de Física, Universidade do Porto, 4150 Porto, Portugal

P.B. Tavares

Departamento de Química, Universidade de Trás-os-Montes e Alto Douro, 5001-911 Vila Real, Portugal

A.M. Gomes and I.S. Oliveira

Centro Brasileiro de Pesquisas Físicas, Rua Dr. Xavier Sigaud 150 Urca, 22290-180 Rio de Janeiro-RJ, Brasil

(Dated: November 9, 2018)

In the present work we analyze the influence of the charge-ordering on the magnetocaloric effect of Pr_{1-x}Ca_xMnO₃ manganites. The results for the samples with $x < 0.30$ present the usual ferromagnetic behavior, peaking at the Curie temperature T_C . In contrast, for the samples above the onset concentration for the charge-ordering ($x \sim 0.30$), an anomalous magnetic entropy change was observed below the charge-ordering temperature T_{CO} , persisting for lower temperatures. This effect is associated to a positive contribution to the magnetic entropy change due to charge-ordering, which is superimposed to the negative contribution from the spin ordering. We found that the charge-ordering component peaks at T_N and is negligible above T_{CO} . Moreover, around T^* (temperature below which the insulator-metal transition induced by magnetic field becomes completely irreversible, where the system remains in such state even after the external magnetic field has been removed), we found extremely large values for the magnetic entropy change, establishing a ‘colossal’ magnetocaloric effect on CMR manganites.

PACS numbers: 75.30.Sg, 75.47.Lx, 75.47.Gk

Keywords: Manganites, magnetocaloric effect, charge ordering

I. INTRODUCTION

The magnetocaloric effect (MCE) is intrinsic to magnetic materials, and is induced via coupling of the magnetic sublattice with the magnetic field, which alters the magnetic part of the total entropy due to a corresponding change of the magnetic field. The MCE can be estimated via the magnetic entropy change $\Delta S_M(T, \Delta H)$, and is a function of both, temperature T and the magnetic field change ΔH , being usually recorded as a function of temperature, at a constant ΔH . In addition, the MCE has a significant technological importance, since magnetic materials with large MCE values could be employed in various thermal devices¹.

The magnetic entropy is related to the magnetization M , magnetic field strength H and absolute temperature T through the Maxwell relation²:

$$\left(\frac{\partial S_M(T, H)}{\partial H}\right)_T = \left(\frac{\partial M(T, H)}{\partial T}\right)_H \quad (1)$$

which after integration yields:

$$\Delta S_M(T, \Delta H) = \int_{H_I}^{H_F} dS_M(T, H)_T = \int_{H_I}^{H_F} \left(\frac{\partial M(T, H)}{\partial T}\right)_H dH \quad (2)$$

Hence, $\Delta S_M(T, \Delta H)$ can be numerically calculated for any temperature, using Eq.2 and the measured magnetization as a function of magnetic field and temperature. Generally, since temperature stabilization is the longest step in the process of collecting magnetization data, the measurements are usually carried out isothermally by varying the magnetic field, for a range of temperature values.

Several authors, through many decades, have studied the magnetocaloric effect in a large variety of magnetic materials. However, more recently, an enormous amount of work^{3,4,5,6,7,8,9,10,11,12,13,14,15,16,17,18} were devoted to explore the MCE in the mixed-valency manganites AMnO₃, where A is a trivalent rare-earth mixed with a divalent alkaline-earth.

Particularly interesting as candidates for technological applications are the $\text{Pr}_{1-x}\text{Ca}_x\text{MnO}_3$ manganites, since their phase diagram exhibit a rich variety of magnetic, electric and crystallographic structures. In this direction, we aim to explore the magnetocaloric effect through the concentration range of phase competition between the antiferromagnetic-insulator-charge-ordered state and ferromagnetic-insulator state, and analyze the influence of the charge ordering on the magnetocaloric properties of these compounds.

Hence, the next section is devoted to a brief survey of the magnetic, electric and crystallographic properties of the $\text{Pr}_{1-x}\text{Ca}_x\text{MnO}_3$ manganites. Following, the section after is dedicated to the experimental details. In section IV a complete description of the experimental results is given, with a thorough discussion and analysis in the following sections.

II. A BRIEF SURVEY

For $x < 0.30$ an orthorhombic O' ($c/\sqrt{2} \lesssim a < b$) crystal structure establishes below 950 K, for $x = 0.0$, and 325 K, for $x \sim 0.30$, whereas for $0.30 < x < 0.75$ the crystal phase arisen is a pseudo-tetragonal compressed T ($c/\sqrt{2} < a$), for temperatures below the onset temperature for the charge-ordering T_{CO} . For high temperatures, the crystal phase is always orthorhombic of O type ($a \simeq b \simeq c/\sqrt{2}$)¹⁹. For $x \sim 0.30$, at low temperatures, a strong crystal phase competition arises between the orthorhombic O' and the pseudo-tetragonal compressed T ¹⁹.

However, the phase coexistence around $x \sim 0.30$ is not limited to the crystallographic aspects, but a remarkable electric²⁰ and magnetic^{21,22,23,24,25,26,27,28,29} phase competition can also be found. In this direction, neutron diffraction²² and muon spin relaxation (μSR)²³ recognized, for $x \sim 0.30$, two magnetic transition, around 140 K and 120 K. The first transition, at higher temperature, corresponds to the antiferromagnetic arrangement, and the other represents an ferromagnetic contribution. Hence, two different interpretations are, in principal, possible: two separated magnetic phases with different critical temperatures, or, alternatively, a collinear-antiferromagnetic phase with T_N at higher temperature, with an additional magnetic transition to a canted-antiferromagnetic structure, at lower temperature. However, de Gennes³⁰ stressed out that an uniform canting can be achieved only in the presence of free carriers, i.e., in a metal, whereas the present system is an insulator. Bound carriers would give rise to a local ferromagnetic distortion of the spin system, which would therefore become inhomogeneous³⁰. In an insulator, the bound electrons would form small ferromagnetic cluster in a antiferromagnetic matrix, and the cluster of spins would then align parallel to each other at T_C ²². Additionally, the presence of the phase boundary between two different crystallographic types (O' and T), lead us to conclude that the coexistence of two phases is more probable than a canted-antiferromagnetic structure. Finally, NMR²⁰, μSR ²³ and neutron diffraction^{19,22}, add and support our suggestion. Thus, this view will be assumed in the further discussions.

For $x < 0.15$, a spin-canted insulator CI phase establishes below 100 K^{19,21,26,28}, whereas for $0.15 < x < 0.30$ a ferromagnetic insulator FMI phase arises, with Curie temperature around 120 K^{21,26,27,28}. For $0.30 < x < 0.80$, an antiferromagnetic-insulator AFMI phase arises for temperatures typically below 170 K^{19,26,27}, coexisting with a charge-ordered CO state with onset temperature T_{CO} between 210 K, for $x = 0.30$, and 170 K, for $x = 0.80$ ²⁷. Additionally, it is well established^{19,22,23} that the clusters embedded in the antiferromagnetic matrix achieve the ferromagnetic order around 110 K, for $x = 0.30$, and 42 K, for $x = 0.40$ ²⁶. In this direction, our recent work using NMR²⁰, gives the ferromagnetic fraction within the antiferromagnetic matrix, as a function of Ca content, x .

For temperatures below than a characteristic temperature T^* , ranging from 60 K for $x = 0.30$ and 20 K for $x = 0.35$ ²⁶, the application of a magnetic field induces a first-order and completely *irreversible* transition to a fully ferromagnetic-metallic FMM state^{21,26,31,32}, where the system remains in such state even after the external magnetic field has been removed. However, for temperature ranges $T^* < T < T_{CO}$, the system return to the insulator state, with hysteresis, after the increase-decreasing magnetic field cycle. The strong hysteresis associated with this transition is indicated by the shaded region in the $H - T$ diagram sketched in figure 1, for $x = 0.35$. Additionally, this insulating state can also be driven metallic by an applied electric field^{33,34}, high pressure³⁵, visible light^{36,37} or x-ray^{22,38}.

However, all values mentioned above are slightly dependent on the sample preparation procedure, and the differences in results can be attributed to the grain size^{12,39,40,41}, oxygen content^{41,42,43,44,45}, vacancy on the lattice⁴⁶, etc. Additionally, the phase diagram presented here (figure 2), is not completely established, since the magnetic structure for several values of Ca concentration x is still a matter of discussion^{21,22,23,24,25,26,27,28,29}.

III. EXPERIMENTAL PROCEDURE

The samples $x = 0.20, 0.25, 0.30, 0.32, 0.35$ and 0.40 , were prepared by the ceramic route, starting from the stoichiometric amount of Pr_2O_3 (99.9 %), CaCO_3 (>99 %) and MnO_2 (>99 %), and heated in air, with five intermediate crushing/pressing steps. The final crushed powders were compressed and sintered in air at 1350 °C during 45 hours,

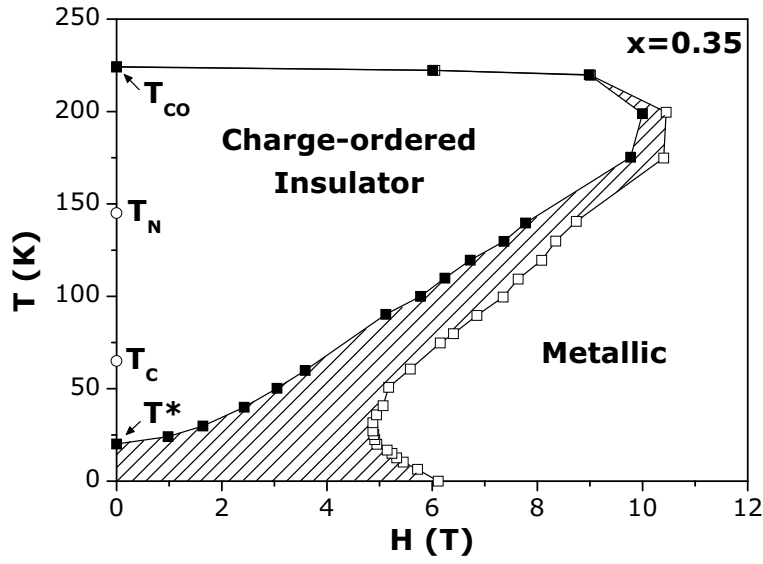


FIG. 1: $H - T$ phase diagram for $\text{Pr}_{1-x}\text{Ca}_x\text{MnO}_3$, with $x = 0.35$. The insulator-metal transition induced by an external magnetic field is reversible, with hysteresis, for temperatures between T_{CO} and T^* , as indicated by the shaded area. Below T^* , the insulator state can also be driven metallic, and kept in this state even after the magnetic field have been removed. After Tomioka *et al.*²⁶.

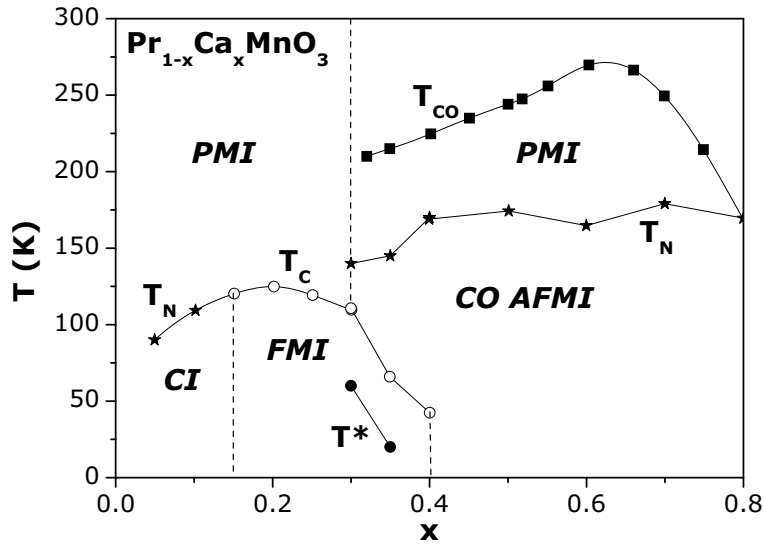


FIG. 2: Magnetic and electric phase diagram for $\text{Pr}_{1-x}\text{Ca}_x\text{MnO}_3$ manganites. *PMI* - paramagnetic insulator; *CI* - spin canted insulator; *FMI* - ferromagnetic insulator; *CO AFMI* - charge-ordered antiferromagnetic insulator.

with a subsequent fast freezing of the samples. X-ray diffraction patterns confirmed that the samples lie in the $Pbnm$ space group, without vestige of spurious phase.

The temperature and external magnetic field dependence of the magnetization were carried out using a commercial SQUID magnetometer. The data were acquired after the sample had been zero-field cooled, under the isothermal regime (M vs. H curves), varying the applied magnetic field from zero up to 50 kOe, and temperature ranges from 10 K up to 400 K. After each M vs. H curve, the sample was heated without the influence of the external magnetic field. For the DC-susceptibility χ_{DC} ($=M/H$ at low field), the measurements were performed at a fixed magnetic field ($H=10$ Oe), sweeping the temperature.

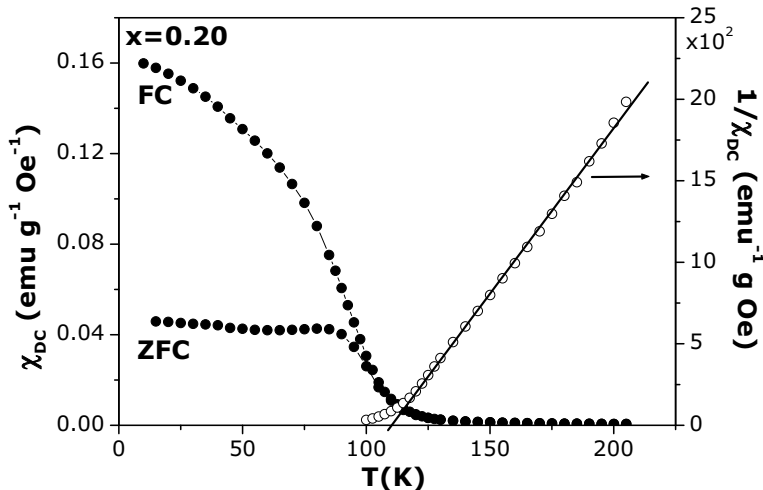


FIG. 3: Left axis: zero-field-cooled (ZFC) and field-cooled (FC) DC-susceptibility χ_{DC} ($=M/H$, with $H=10$ Oe) as a function of temperature, for $x=0.20$. Right axis: temperature dependence of the inverse of the DC-susceptibility.

IV. RESULTS

In this section we will describe the field and temperature dependence of the magnetization $M(T,H)$, since it is one of the best experimental tools to understand the magnetocaloric potential of the system under study.

The zero-field-cooled (ZFC) and field-cooled (FC) DC-susceptibility χ_{DC} ($=M/H$, with $H=10$ Oe), were measured for all samples available. We observed a similar behavior for those below the onset concentration for charge ordering ($x \sim 0.30$), with a well defined transition from the paramagnetic to the ferromagnetic phase. While the DC-susceptibility χ_{DC} , after field cooling, increase with decreasing temperature, after the sample had been zero-field-cooled, it keeps an almost temperature independence feature. Additionally, from the quantity $1/\chi_{DC}$, we could observe the usual Curie-Weiss law, allowing to estimate the value of the paramagnetic effective moment p_{eff} and the paramagnetic Curie temperature θ_p . Thus, figure 3 sketched the behavior above described, representative for all samples $x < 0.30$.

On other hand, for $x > 0.30$ the DC-susceptibility change its slope when the sample is cooled down through the CO transition, implying in two different Curie-Weiss law, depending on the temperature range: one for $T > T_{CO}$ and other for $T_N < T < T_{CO}$. This behavior, already reported²³, is illustrated in figure 4, for $x = 0.40$. In addition, a well defined transition from the paramagnetic phase to the antiferromagnetic phase are also observed, as well as the characteristic temperature T^* , below which the field-induced insulator-metal transition is completely irreversible (see section II). The quantities obtained from the analysis of the DC-susceptibility are summarized on table I. Figure 5 sketched the concentration dependence of (a) the paramagnetic Curie temperature θ_p and (b) the paramagnetic effective moment p_{eff} . The two branches curve displayed is consequence of the two Curie-Weiss law found for $x > 0.30$.

The temperature and field dependence of the magnetization $M(T,H)$ were also measured for all samples. From the data analysis of the several M vs. H isotherms, we could build the curves for the thermal dependence of the magnetization, at a fixed magnetic field. For $x = 0.20$, as the temperature is further decreased, one observes that the magnetization starts to increase faster below 100 K, peaking at around 35 K, as displayed in figure 6(a). It can be related to the vicinity of this sample to the onset concentration to spin-canted order ($x < 0.15$)^{21,26}. On the other hand, for $x = 0.25$ and 0.30 an usual behavior for the thermal dependence of the magnetization is found, as in figure 6(b).

However, for Ca concentration x above the onset concentration for charge ordering ($x \sim 0.30$), the temperature dependence of the magnetization have interesting features. For $x = 0.32$, for instance, the two peaks around 220 K and 130 K correspond to the establishment of the charge ordering and the antiferromagnetic spin ordering, respectively, in accordance with several works^{21,26}, including those using neutron diffraction^{19,22,47,48}. As the temperature is further decreased, we can verify a remarkable increasing of the magnetization below 50 K, peaking at around $T^*=26$ K, with a subsequent lost of magnetic moment, reaching 40 emu/g at 5 K and 40 kOe. A similar behavior had been found for all samples with $x > 0.30$. This features, that can be seen in figure 7 for (a) $x = 0.32$ and (b) $x = 0.40$, was already observed for $x = 0.37$ ²⁵.

For all measurements, when the magnetic field is turned off, it oscillates around zero field in order to avoid residual

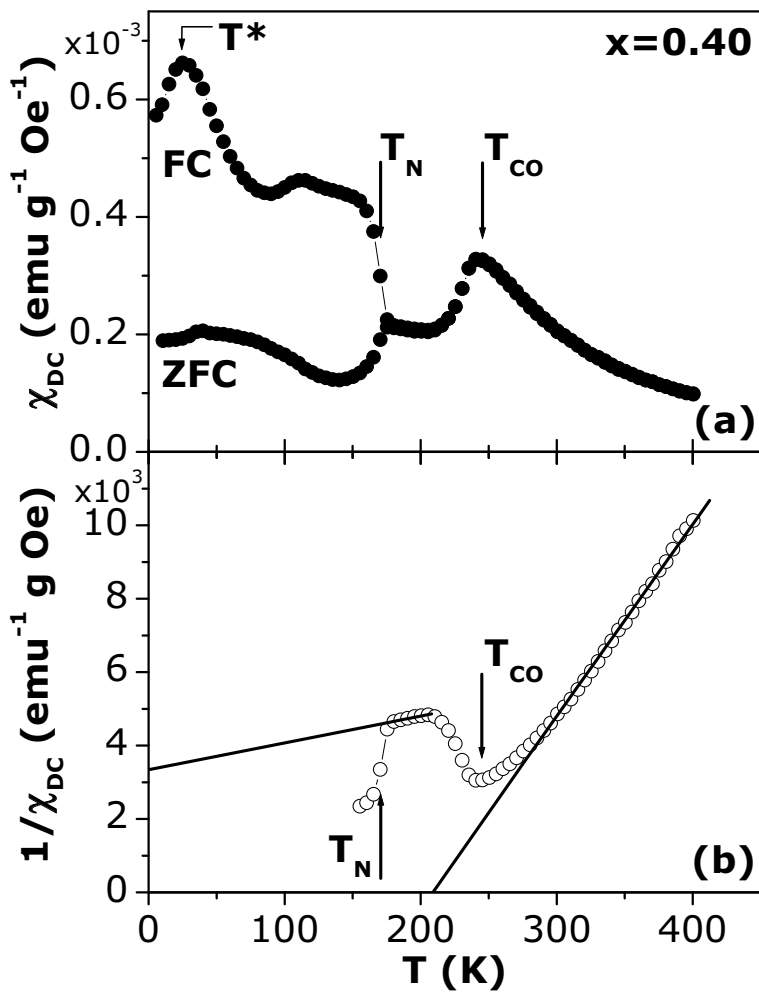


FIG. 4: (a) Temperature dependence of the zero-field-cooled (ZFC) and field-cooled (FC) DC-susceptibility χ_{DC} ($=M/H$, with $H=10$ Oe), for $x = 0.40$. (b) Temperature dependence of the inverse of the DC-susceptibility, with two distinct Curie-Weiss law: one for $T > T_{CO}$, and other for $T_N < T < T_{CO}$.

field to the next M vs. H curve. If this procedure is not performed, a remarkable difference is found for the magnetization values at low temperatures. The M vs. T curves also peaks around $T^* = 26$ K, although keeps a high magnetization value for temperature below the peak (80 emu/g for 5 K and 40 kOe). This feature can be seen in the inset of the figure 7(a).

Following, the next section is devoted to analyze the influence of the charge-ordering on the magnetocaloric effect, which will be derived from the magnetization data, using Eq.2.

V. INFLUENCE OF THE CHARGE-ORDERING ON THE MAGNETOCALORIC EFFECT

In the previous sections, we provided detailed information referred to the magnetic properties of the $\text{Pr}_{1-x}\text{Ca}_x\text{MnO}_3$ manganites. The aim of this section is the discussion concerning the analysis of the magnetocaloric potential of these manganites, obtained from the previously presented magnetic data.

A. MCE around T_{crit}

The magnetic entropy change $\Delta S_M(T)$ can be estimated using Eq.2, and are sketched in figure 8 for all samples available ($x = 0.20; 0.25; 0.30; 0.32; 0.35; 0.40$).

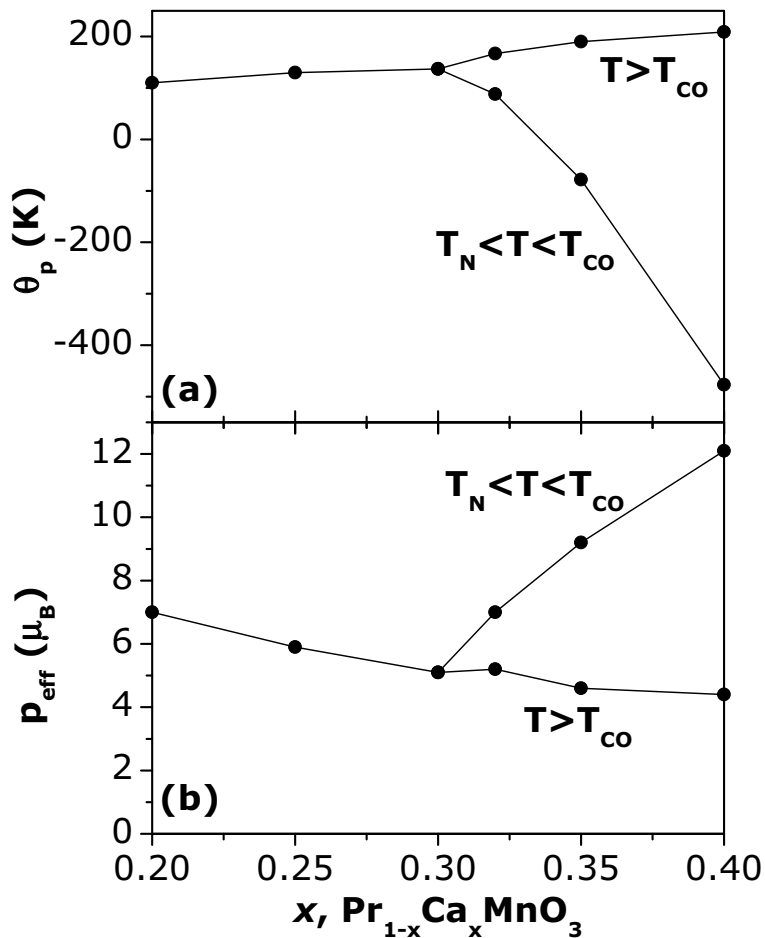


FIG. 5: (a) Paramagnetic Curie temperature θ_p and (b) paramagnetic effective moment p_{eff} as a function of Ca content, x .

For $x=0.20$, the magnetic entropy change has an usual behavior for temperatures above 100 K, where the magnetization data (figure 6(a)) has also a well shaped feature. However, below 100 K, the magnetization starts to increase faster as the temperature is further decreased, as already discussed in Section IV, and it is possibly related to the closed vicinity of this sample to the spin-canted structure that arise below $x=0.15$ ^{19,21,26,28} (see figure 2). Thus, the anomalous behavior found for $T < 100$ K on the magnetic entropy change of $x=0.20$ can also be explained considering the influence of the spin-canted structure. On the other hand, for $x=0.25$ and 0.30 , concentrations completely embedded within the ferromagnetic region, a very usual behavior for ΔS_M are found for both, as sketched in figure 8. We consider, in the case of $x=0.25$ and 0.30 , that the contribution to the magnetic entropy change is purely due to the spin magnetic moment of the sample. However, for samples with concentrations above $x \sim 0.30$, the charge-ordering arrangement plays a decisive role. When the temperature is further decreased, the magnetic entropy change ΔS_M follows an usual shape until reach the onset temperature for the charge-ordering T_{CO} , below which such behavior is completely broken, as can be observed in figure 8.

To analyze this intriguingly feature, we consider two different contributions to the total magnetic entropy change ΔS_M : one refers to the spin rearrangement ΔS_{spin} , and the other concerns to the charge ordering rearrangement ΔS_{CO} , as follow:

$$\Delta S_M = \Delta S_{spin} + \Delta S_{CO} \quad (3)$$

Thus, considering that the spin contribution to the total magnetic entropy change of $x > 0.30$ is almost similar to the purely spin contribution of $x = 0.30$, shifted to its T_{crit} , we can satisfactorily estimate the charge-ordering contribution. Thus, figure 9 presents the CO and spin contribution to the total magnetic entropy change ΔS_M , for (a) $x=0.32$, (b) 0.35 and (c) 0.40 .

The behavior of the positive charge-ordering contribution, that peaks at T_N , can be understood as follow. For $T_N < T < T_{CO}$, i.e., in the paramagnetic phase, the applied magnetic field force a rude alignment of the spins, increasing the Mn^{3+} - Mn^{4+} electron hopping and decreasing the concentration of Mn^{3+} - Mn^{4+} charge-ordered, when compared with the zero field case. Consequently, the entropy due the CO increase under an external applied magnetic field, allowing an positive CO entropy change. However, for temperatures immediately below T_N , the applied magnetic field favors the increasing of the antiferromagnetic spin arrangement, comparing to the case without field, and, consequently, the decreasing of the Mn^{3+} - Mn^{4+} electron mobility. Thus, the concentration of Mn^{3+} - Mn^{4+} charge-ordered increases, implying in the decreasing of the entropy change due the charge-order, under an applied magnetic field.

The magnetic entropy change for several values of magnetic field change (ΔH : 0 \rightarrow 1; 2; 3 and 4 T) are sketched in figure 10, for $x = 0.32$. Both contributions: charge-order (estimated) and spin ($x = 0.30$), follow the usual magnetic field dependence.

B. MCE around T^*

The larger values of magnetic entropy change were obtained around T^* , where, again, the charge-ordering features found in these manganites plays a decisive role to the MCE (see figure 1). The value of ΔS_M vanishes exactly at T^* , being highly negative (positive) for higher (lower) temperatures. For $x = 0.32$, for instance, ΔS_M reach $-19.4 \text{ J kg}^{-1} \text{ K}^{-1}$ at 32 K, and $13.4 \text{ J kg}^{-1} \text{ K}^{-1}$ at 14 K. Figure 11 sketched these features for $x = 0.32, 0.35$ and 0.40 , under 4 T of magnetic field change. For the sake of clearness, table II presents the larger values of ΔS_M found in these samples, comparing with reported values of others metals and manganites.

However, the positive ΔS_M below T^* can assume different values, depending on the process in which the magnetization data were obtained. As already discussed in section IV, the M *vs.* T curves, build from several M *vs.* H curves, have different features depending if the experimental setup performs or not a magnetic field oscillation, around zero field, to avoid residual field on the coils for the next M *vs.* H curve (see figure 7(a)). Thus, figure 12 presents the magnetic entropy change, under 4 T of magnetic field change and $x = 0.32$, with both cases: *with* and *without* the oscillating magnetic field. For the last case, the positive ΔS_M is almost suppressed, and this feature are probably related to the metallic state in which is the sample (for $T < T^*$), since an applied magnetic field induce a completely irreversible insulator-metal transition for temperatures below T^* , as already discussed in section II.

The temperature dependence of the magnetic entropy change has an usual tendency with respect to several values of magnetic field change, as presented in figure 13, for $x = 0.32$ and ΔH : 0 \rightarrow 1; 2; 3 and 4 T.

VI. CONCLUSION

In the present work, we found an anomalous magnetic entropy change for $x > 0.30$ (concentrations exhibiting charge-ordering phenomenon). The results could be explained considering a spin and charge-ordering contributions to the total magnetic entropy change. Moreover, we found an extremely large value for the entropy variation, that occurs

TABLE I: Values obtained for T^* , the onset temperature below which the field-induced insulator-metal transition is completely irreversible; T_{CO} , charge-ordering temperature; the critical temperature T_{crit} , obtained form the maximum of $d\chi_{DC}/dT$; θ_p , the paramagnetic Curie temperature; and, finally, p_{eff} , the paramagnetic effective moment.

x	T^* (K)	T_{CO} (K)	T_{crit} (K)	θ_p (K)	p_{eff} (μ_B)
0.20	-	-	100 ^a	110	7.0
0.25	-	-	120 ^a	130	5.9
0.30	-	-	128 ^a	137	5.1
0.32	26	210	113 ^b	88 ^c	7.0 ^c
				167 ^d	5.2 ^d
0.35	19	222	152 ^b	-78 ^c	9.2 ^c
				190 ^d	4.6 ^d
0.40	11	244	170 ^b	-477 ^c	12.1 ^c
				209 ^d	4.4 ^d

^aCurie temperature

^bNéel temperature

^c $T_N < T < T_{CO}$

^d $T > T_{CO}$

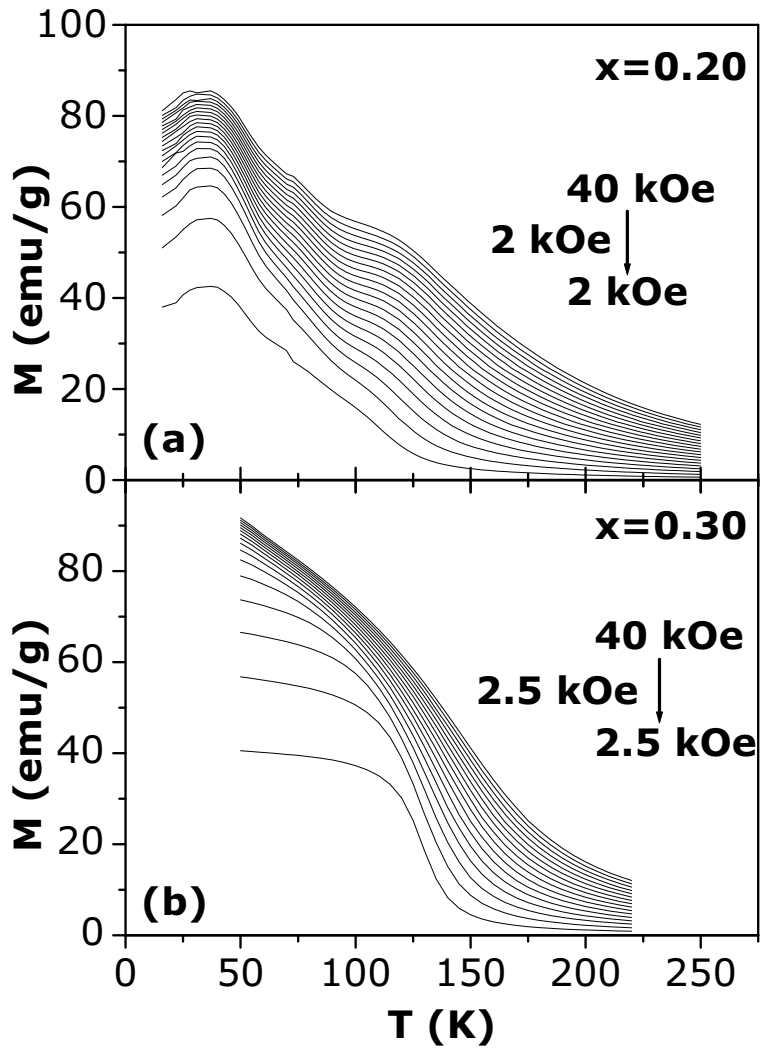


FIG. 6: Temperature dependence of the magnetization data, for (a) $x = 0.20$ and (b) $x = 0.30$. The graphic was built from the measured M vs. H curves, for several temperatures.

TABLE II: Comparison of reported values of the maximum magnetic entropy change of metals and manganites.

Material	$-\Delta S_M$ ($J\ kg^{-1}\ K^{-1}$)	ΔH (kOe)	T_C (K)	Ref.
$La_{0.67}Ca_{0.33}MnO_3$	6.4	30	267	[4]
$La_{0.60}Y_{0.07}Ca_{0.33}MnO_3$	1.5	30	230	[7]
$La_{0.80}Ag_{0.20}MnO_3$	3.4	30	270	[49]
$Pr_{0.60}Ca_{0.40}MnO_3$	4.3	40	13^c	present work
$Pr_{0.65}Ca_{0.35}MnO_3$	20.1	40	21^c	present work
$Pr_{0.68}Ca_{0.32}MnO_3$	19.4	40	32^c	present work
Dy	19.5	65	174	[50]
Gd	7.1	30	294	[51]
$Gd_{0.73}Dy_{0.27}$	10	50	265	[52]
$Gd_5(Si_2Ge_2)^a$	7	50	300	[53]
$Gd_5(Si_2Ge_2)^b$	14	20	276	[53]

^aPrepared using commercial purity Gd (95-98% pure)

^bPrepared using high purity Gd (~99.8% pure)

^cAround T^* , instead T_C

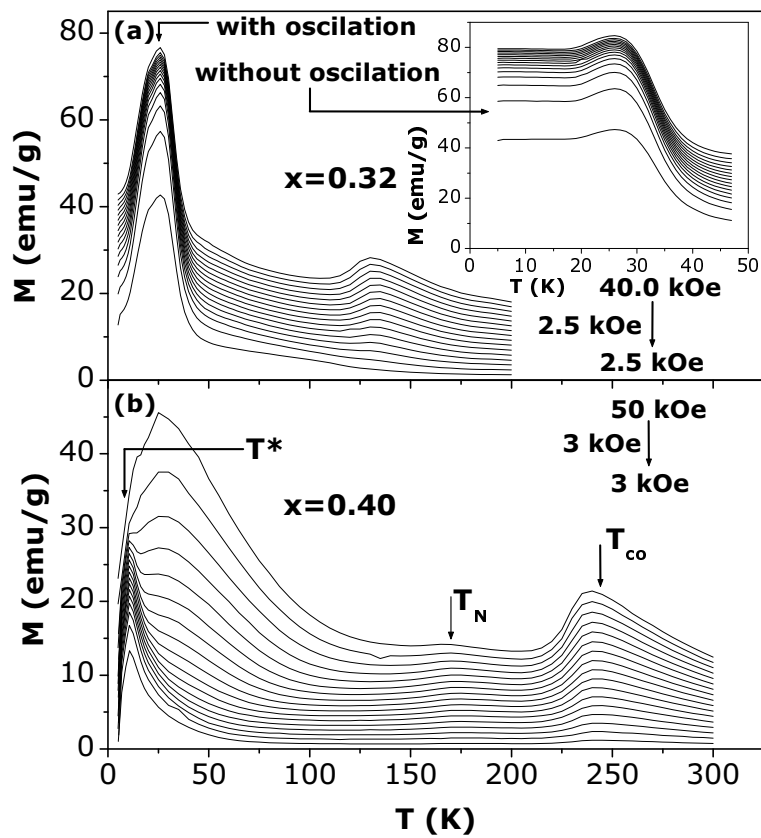


FIG. 7: Temperature dependence of the magnetization data, for (a) $x=0.32$ and (b) $x=0.40$. The graphic was built from the measured M vs. H curves. For all measurements, when the magnetic field is turned off, it oscillates around zero field in order to avoid residual field to the next M vs. H curve, except for the data presented in the inset.

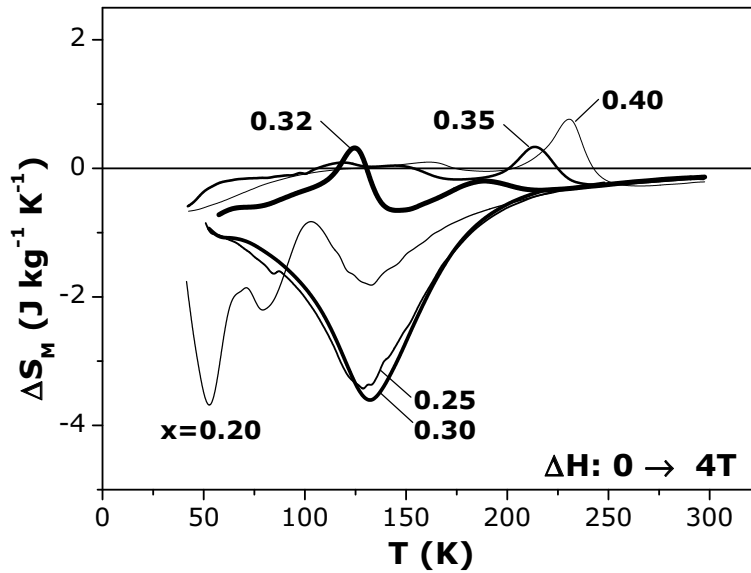


FIG. 8: Temperature dependence of the magnetic entropy change, around T_{crit} , under 4 T of magnetic field change, for $x=0.20$; 0.25; 0.30; 0.32; 0.35 and 0.40.

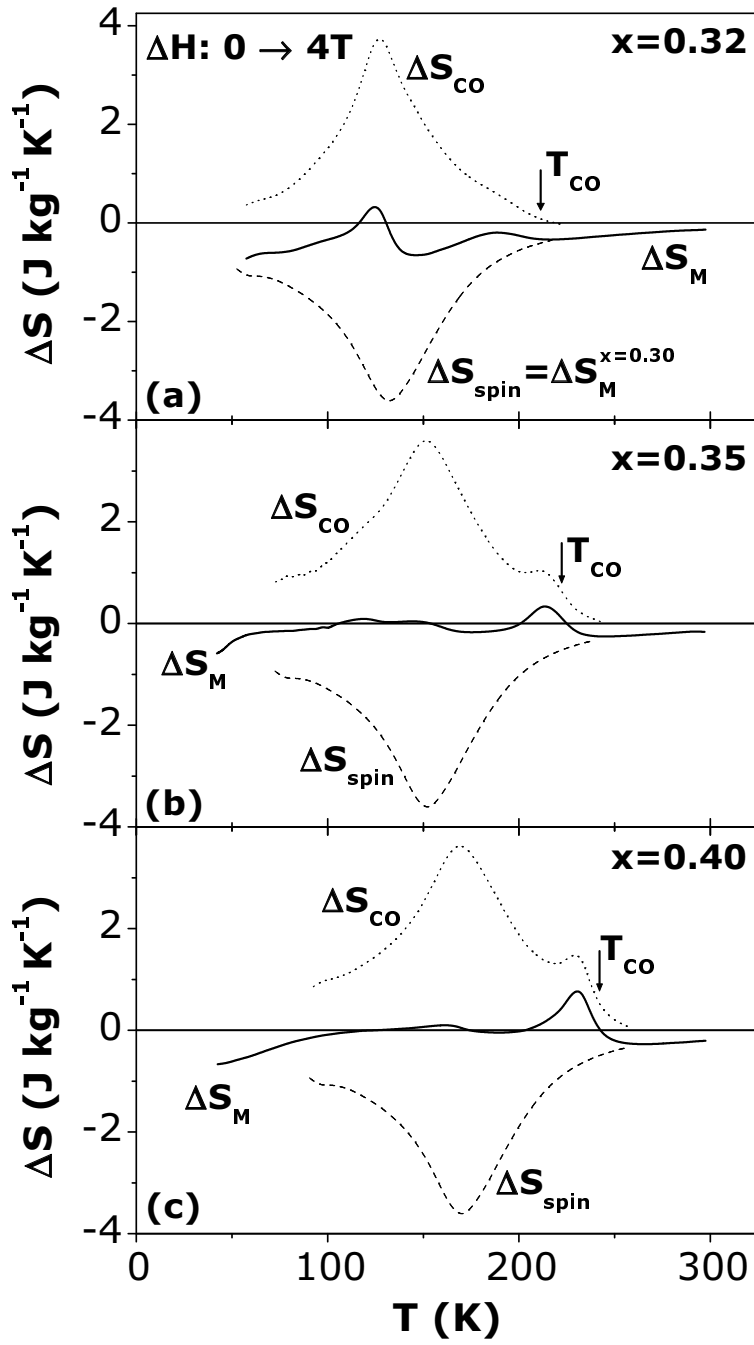


FIG. 9: Spin contribution ΔS_{spin} and charge-ordering contribution ΔS_{co} to the total magnetic entropy change ΔS_{M} , for (a) $x = 0.32$, (b) $x = 0.35$, and (c) $x = 0.40$, and under 4 T of magnetic field change.

at a characteristic temperature T^* . Other manganites showing the characteristic temperature T^* (see ref.³²), can also present large magnetic entropy change, and, consequently, a great potential to be employed in various thermal devices.

In some previous publications^{54,55,56} we pointed out that the unusual properties of manganites result from their magnetic non-extensivity, in the sense of Tsallis statistics⁵⁷. Such an approach is being applied to the analysis of the present results and will be published elsewhere.

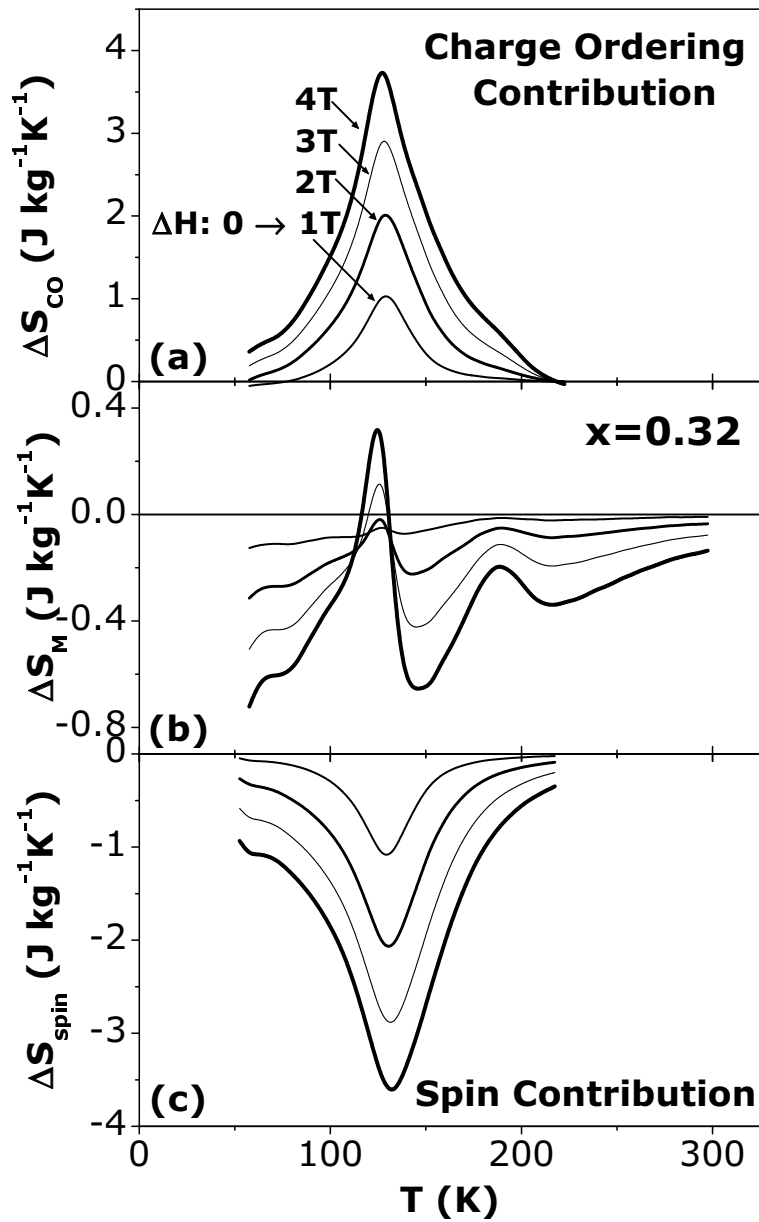


FIG. 10: Temperature dependence of the (a) charge-ordering contribution ΔS_{CO} and (c) spin contribution ΔS_{spin} to the (b) total magnetic entropy change ΔS_M , under several values of magnetic field change and $x = 0.32$.

Acknowledgments

The authors thanks FAPERJ/Brasil, FCT/Portugal (contract POCTI/CTM/35462/99) and ICCTI/CAPES (Portugal-Brasil bilateral cooperation), for financial support.

* Electronic address: marior@fis.ua.pt

¹ V. K. Pecharsky and K. A. Gschneidner, J. Appl. Phys. **86**, 565 (1999).

² A. H. Morrish, *The Physical Principles of Magnetism* (Wiley, New York, 1965), chap. 3.

³ Y. Sun, W. Tong, N. Liu, and Y. Zhang, J. Magn. Magn. Mater. **238**, 25 (2002).

⁴ Y. Sun, X. Xu, and Y. Zhang, J. Magn. Magn. Mater. **219**, 183 (2000).

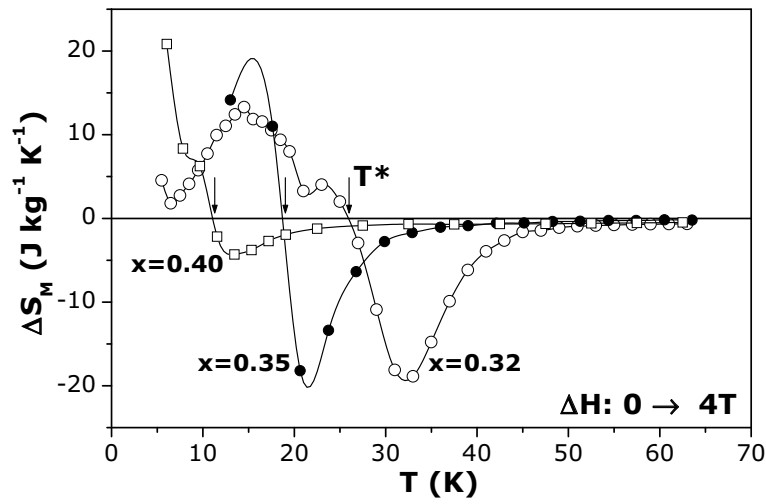


FIG. 11: Magnetic entropy change around T^* as a temperature function for $x=0.32, 0.35$ and 0.40 , under 4 T of magnetic field change.

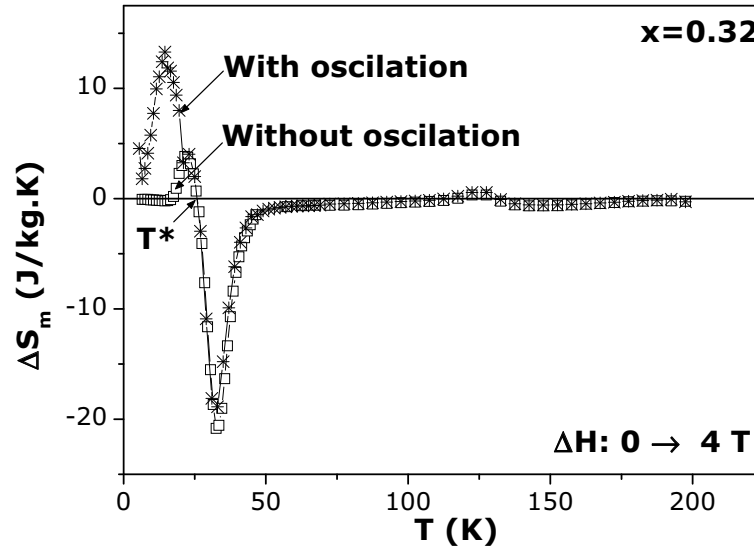


FIG. 12: Temperature dependence of the magnetic entropy change around T^* , for $x=0.32$ and under 4 T of magnetic field change. The two cases represent *with* and *without* oscillating magnetic field after each M vs. H curve.

- ⁵ Z. M. Wang, G. Ni, Q. Y. Xu, H. Sang, and Y. W. Du, J. Appl. Phys. **90**, 5689 (2001).
- ⁶ G. Gu, J. Cai, W. Yang, and Y. Du, J. Appl. Phys. **84**, 3798 (1998).
- ⁷ X. X. Zhang, J. Tajada, Y. Xin, G. F. Sun, K. W. Wong, and X. Bohigas, Appl. Phys. Lett. **69**, 3596 (1996).
- ⁸ M. S. Reis, J. C. C. Freitas, M. T. D. Orlando, A. M. Gomes, A. L. Lima, I. S. Oliveira, A. P. Guimaraes, and A. Y. Takeuchi, J. Magn. Magn. Mater. **242**, 668 (2002).
- ⁹ Y. Xu, U. Memmert, and U. Hartmann, J. Magn. Magn. Mater. **242**, 698 (2002).
- ¹⁰ P. Chen, Y. W. Du, and G. Ni, Europhys. Lett. **52**, 589 (2000).
- ¹¹ J. Mira, J. Rivas, L. E. Hueso, F. Rivadulla, and M. A. López-Quintela, J. Appl. Phys. **91**, 8903 (2002).
- ¹² L. E. Hueso, P. Sande, D. R. Miguéns, J. Rivas, F. Rivadulla, and M. A. López-Quintela, J. Appl. Phys. **91**, 9943 (2002).
- ¹³ D. T. Morelli, A. M. Mance, J. V. Mantese, and A. L. Micheli, J. Appl. Phys. **79**, 373 (1996).
- ¹⁴ A. Szewczyk, H. Szymczac, A. Wisniewski, K. Piotrowski, R. Kartaszynski, B. Dabrowski, S. Kolesnik, and Z. Bukowski, Appl. Phys. Lett. **77**, 1026 (2000).
- ¹⁵ Z. B. Guo, Y. W. Du, J. S. Zhu, H. Huang, W. P. Ding, and D. Feng, Phys. Rev. Lett. **78**, 1142 (1997).
- ¹⁶ H. Huang, Z. B. Guo, D. H. Wang, and Y. W. Du, J. Magn. Magn. Mater. **173**, 302 (1997).
- ¹⁷ X. Bohigas, J. Tejada, E. del Barco, X. X. Zhang, and M. Sales, Appl. Phys. Lett. **73**, 390 (1998).

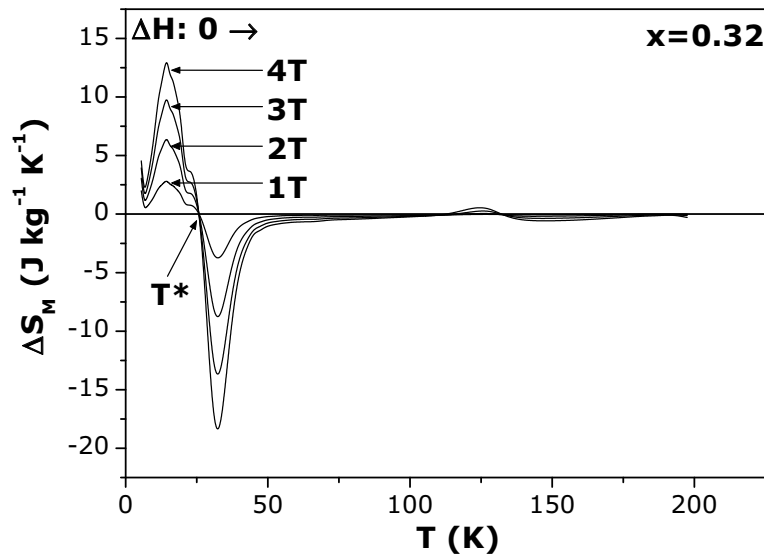


FIG. 13: Temperature dependence of the magnetic entropy change around T^* , for $x = 0.32$, under several values of magnetic field change, and for the case with oscillating magnetic field after each M vs. H curve.

- ¹⁸ X. Bohigas, J. Tejada, M. L. Marínez-Sarrión, S. Tripp, and R. Black, *J. Magn. Magn. Mater.* **208**, 85 (2000).
- ¹⁹ Z. Jirák, S. Krupicka, Z. Simsa, M. Dlouhá, and S. Vratislav, *J. Magn. Magn. Mater.* **53**, 153 (1985).
- ²⁰ M. S. Reis, V. S. Amaral, P. B. Tavares, A. M. Gomes, A. Y. Takeuchi, A. P. Guimaraes, I. S. Oliveira, and P. Panissod (2003), cond-mat/0211143.
- ²¹ Y. Tokura, Y. Tomioka, H. Kuwahara, A. Asamitsu, Y. Moritomo, and M. Kasai, *J. Appl. Phys.* **79**, 5288 (1996).
- ²² D. E. Cox, P. G. Radaelli, M. Marezio, and S. W. Cheong, *Phys. Rev. B* **57**, 3305 (1998).
- ²³ C. Frontera, J. L. García-Muñoz, A. Llobet, M. Respaud, J. M. Broto, J. S. Lord, and A. Planes, *Phys. Rev. B* **62**, 3381 (2000).
- ²⁴ M. Roy, J. F. Mitchell, A. P. Ramirez, and P. Schiffer, *Phys. Rev. B* **62**, 13876 (2000).
- ²⁵ V. Hardy, A. Wahl, C. Martin, and C. Simon, *Phys. Rev. B* **63**, 224403 (2001).
- ²⁶ Y. Tomioka, A. Asamitsu, H. Kuwahara, Y. Moritomo, and Y. Tokura, *Phys. Rev. B* **53**, R1689 (1996).
- ²⁷ C. Martin, A. Maignan, M. Hervieu, and B. Raveau, *Phys. Rev. B* **60**, 12191 (1999).
- ²⁸ J. P. Renard and A. Anane, *Materials Science and Engineering B* **63**, 22 (1999).
- ²⁹ M. Roy, J. F. Mitchell, A. P. Ramirez, and P. Schiffer, *Philosophical Magazine B* **81**, 417 (2001).
- ³⁰ P. G. de Gennes, *Phys. Rev.* **118**, 141 (1960).
- ³¹ Y. Tomioka, A. Asamitsu, Y. Moritomo, and Y. Tokura, *J. Phys. Soc. Jpn.* **64**, 3626 (1995).
- ³² Y. Tokura and Y. Tomioka, *J. Magn. Magn. Mater.* **200**, 1 (1999).
- ³³ A. Asamitsu, Y. Tomioka, H. Kuwahara, and Y. Tokura, *Nature* **388**, 50 (1997).
- ³⁴ J. Stankiewicz, J. Sese, J. Garcia, J. Blasco, and C. Rillo, *Phys. Rev. B* **61**, 11236 (2000).
- ³⁵ Y. Morimoto, H. Kuwahara, Y. Tomioka, and Y. Tokura, *Phys. Rev. B* **55**, 7549 (1997).
- ³⁶ M. Fiebig, K. Miyano, Y. Tomioka, and Y. Tokura, *Science* **280**, 12 (1998).
- ³⁷ K. Miyano, T. Tanaka, Y. Tomioka, and Y. Tokura, *Phys. Rev. Lett.* **78**, 4257 (1997).
- ³⁸ V. Kiryukhin, D. Casa, J. P. Hill, B. Keimer, A. Vigliante, Y. Tomioka, and Y. Tokura, *Nature* **386**, 813 (1997).
- ³⁹ J. Rivas, L. E. Hueso, A. Fondado, F. Rivadulla, and M. A. López-Quintela, *J. Magn. Magn. Mater.* **221**, 57 (2000).
- ⁴⁰ P. Levy, F. Parisi, G. Polla, D. Vega, G. Leyva, H. Lanza, R. S. Freitas, and L. Ghivelder, *Phys. Rev. B* **62**, 6437 (2000).
- ⁴¹ L. E. Hueso, F. Rivadulla, R. D. Sánchez, D. Caeiro, C. Jardón, C. Vázquez-Vázquez, J. Rivas, and M. A. López-Quintela, *J. Magn. Magn. Mater.* **189**, 321 (1998).
- ⁴² J. F. Mitchell, D. N. Argyriou, C. D. Potter, D. G. Hinks, J. D. Jorgensen, and S. D. Bader, *Phys. Rev. B* **54**, 6172 (1996).
- ⁴³ J. Alonso, E. Herrero, J. M. Gonzalez-Calbet, M. Vallet-Regi, J. L. Martinez, J. M. Rojo, and A. Hernando, *Phys. Rev. B* **62**, 11328 (2000).
- ⁴⁴ H. L. Ju and H. Sohn, *J. Magn. Magn. Mater.* **167**, 200 (1997).
- ⁴⁵ S. V. Trukhanov, I. O. Troyanchuk, F. P. Korshunov, V. A. Sirenko, H. Szymczak, and K. Baerner, *Low Temp. Phys.* **27**, 283 (2001).
- ⁴⁶ G. Allodi, R. DeRenzi, and G. Guidi, *Phys. Rev. B* **57**, 1024 (1998).
- ⁴⁷ M. R. Lees, J. Barratt, G. Balakrishnan, D. M. Paul, and C. Ritter, *Phys. Rev. B* **58**, 8694 (1998).
- ⁴⁸ H. Yoshizawa, H. Kawano, Y. Tomioka, and Y. Tokura, *Phys. Rev. B* **52**, 13145 (1995).
- ⁴⁹ T. Tang, K. M. Gu, Q. Q. Cao, D. H. Wang, S. Y. Zhang, and Y. W. Du, *J. Magn. Magn. Mater.* **222**, 110 (2000).
- ⁵⁰ M. Foldeaki, R. Chahine, and T. K. Bose, *J. Appl. Phys.* **77**, 3528 (1995).

- ⁵¹ S. Y. Dan'kov, A. M. Tishin, V. K. Pecharsky, and K. A. Gschneidner, Phys. Rev. B **57**, 3478 (1998).
- ⁵² V. K. Pecharsky and K. A. Gschneidner, Appl. Phys. Lett. **70**, 3299 (1997).
- ⁵³ K. A. Gschneidner and V. K. Pecharsky, J. Appl. Phys. **85**, 5365 (1999).
- ⁵⁴ M. S. Reis, J. C. C. Freitas, M. T. D. Orlando, E. K. Lenzi, and I. S. Oliveira, Europhys. Lett. **58**, 42 (2002).
- ⁵⁵ M. S. Reis, J. P. Araújo, V. S. Amaral, E. K. Lenzi, and I. S. Oliveira, Phys. Rev. B **66**, 134417 (2002).
- ⁵⁶ M. S. Reis, V. S. Amaral, J. P. Araújo, and I. S. Oliveira, Phys. Rev. B (2003), in press - available at cond-mat/0301239.
- ⁵⁷ C. Tsallis, R. S. Mendes, and A. R. Plastino, Physica A **261**, 534 (1998).